Properties of layered double hydroxide micro- and nanocomposites

L. Moyo[1], W.W. Focke[1], D. Heidenreich[2], F.J.W.J. Labuschagne[1] and H.-J. Radusch[2]

[1]Institute of Applied Materials, Department of Chemical Engineering, University of Pretoria, Private Bag X20, Hatfield, 0028, Pretoria, South Africa

[2]Centre of Engineering Science, Martin Luther University Halle-Wittenberg, D-06099 Halle, Germany

Abstract

Carbonate and stearate intercalated layered double hydroxides were used as fillers to prepare polymer micro- and nano-composites respectively. The stearate modified starting material was a bilayer-intercalated clay. During melt compounding excess stearates were released and the clay reverted to a monolayer-intercalated form. The exuded stearate acted as a lubricant lowering the melt viscosity of poly(ethylene-co-vinyl acetate) and linear low density polyethylene matrices. Strong hydrogen bond interactions between the chains of poly(ethylene-co-vinyl alcohol) and the clay platelet surfaces overwhelmed the lubricant effect and caused an increase in the melt viscosity of this matrix. The notched Charpy impact strength of this composite was almost double that of the neat polymer. It appears that this can be attributed to the ability of the highly dispersed and randomly dispersed nano-sized clay platelets to promote extensive internal micro-cavitation during impact loading. This creation of a large internal surface area provided the requisite energy dissipation mechanism.

KEYWORDS: A. Layered compounds, A. Composites, B. Intercalation reactions, C. Electron microscopy, D. Mechanical properties

* Corresponding author. Tel.: +27 12 420 3728; Fax: +27 12 420 2516.
E-mail address: walter.focke@up.ac.za (W.W. Focke)

1. Introduction

It is well-established that dispersion of particles with high aspect ratios such as fibres and platelets in polymeric matrices improves mechanical stiffness as well as some other properties. However, good interfacial adhesion and a homogeneous dispersion are prerequisites [Pradhan et al. 2008]. Nanostructured clays are ideal for the preparation of polymer-clay nanocomposites that exhibit improved gas barrier properties, better mechanical properties [Hsuesh & Chen 2003, Wang et al. 2006], enhanced flame retardancy [Chen & Qu 2003, Chen & Qu 2004, Zammarano *et al.* 2005, Costa et al. 2005, Zubitur 2009], UV and photo-stability [Bocchini *et al.* 2008], ease of photo prodegradability [Magagula *et al*. 2009], etc. In this regard smectite-based polymer composites have attracted much attention [Paul & Robeson 2008]. Just like layered silicates, layered double hydroxides (LDHs) also possess a layered structure and therefore provide an alternative route to the preparation of polymer nanocomposites [Costa et al. 2005, Manhique et al. 2012]

LDHs have the general formula $[M^{2+}_{(1-x)}M^{3+}_{x}(OH)_2\ ]_x(A^{n-}_{(x/n)}).mH_2O$ where A represents a suitable anion, M^{2+} = Mg, Zn, Fe, Co, Ni, Cu and M^{3+} = Al, Fe, Cr, Mn, etc. The crystallography of these clays is similar to that of the mineral hydrotalcite ($Mg_6Al_2(OH)_{16}(CO_3).4H_2O$) [Reichle 1986]. They have a brucite-like structure of stacked sheets in which some trivalent cations isomorphously replaced some of the divalent ones. The net positive charge on the sheets is counterbalanced by exchangeable anions located in the interlayer. Exchanging the anions within the interlayer with others modifies the interlayer properties. For example, the surface energy is lowered and changes from hydrophilic to hydrophobic when fatty acids are intercalated [Nhlapo et al. 2008]. The basal spacing may increase to accommodate polymer chains during intercalation and exfoliation. LDHs are synthetic clays and hence their purity can be controlled in contrast to their natural cationic counterparts. A wide composition range is accessible by using different metal ion pair species

and varying their mole ratio. This means that LDHs can be tailored to fit the required functionality.

IUPAC defines a composite as 'a multicomponent material comprising multiple different (non-gaseous) phase domains in which at least one is a continuous phase' [Work et al. 2004]. Polymer-clay composites can be prepared in three different ways, namely *in-situ* polymerisation [Huang *et al*. 2011, Lee & Im 2007, Moujahid *et al*. 2002], solution intercalation [Ramaraj et al. 2010] and dispersion by melt-processing [Zammarano *et al*. 2006]. Three organo-clay nanocomposites microstructures are possible, i.e. phase separated; intercalated and exfoliated. The outcome is determined by which one of the interfacial interaction is favoured in the system. The three main interactions are polymer-surface, polymer-surfactant and surfactant-surface [Vaia and Giannelis 1997]. The consensus is that, for thorough clay sheet dispersion, highly favourable polymer-surface interactions are essential [Vaia and Giannelis 1997, Fischer 2003].

Exfoliation of surfactant intercalated LDHs has been noted [Leroux *et al.* 2001, Khan and O'Hare 2002, Fischer 2003]. A greater degree of exfoliation and better dispersion of LDHs was obtained in more polar matrices. Polyolefin nanocomposites are difficult to prepare as the low polymer polarity does not provide effective interaction with LDHs. Adding the compatibilizer maleic anhydride grafted polyethylene (PE-g-MA), to some extent, improved dispersion of LDHs in non-polar matrices during melt compounding [Costa *et al.* 2005]. Solution intercalation yields full exfoliation in this system [Chen *et al*. 2003, Chen et al. 2004] and in polystyrene/ZnAl LDH composites [Qui et al. 2005]. However, nanocomposite formation was achieved via melt blending in LDH/PMMA composites [Nyambo *et al.* 2009].

The interlayer anions in surfactant intercalated LDHs show thermotropic behaviour [Nhlapo *et al.* 2008, Focke *et al.* 2010, Moyo *et al.* 2012]. LDH-fatty acids intercalated above the AEC levels apparently melt below polymer processing temperatures (120°C) [Nhlapo *et al.*, 2008]. Droplet formation was observed in hot stage optical microscopy giving a façade of a

completely molten LDH-St [Nhlapo et al. 2008]. This can be attributed to the excess stearate acid exuding and forming a liquid droplet that surrounds the parent LDH-St platelets. However, droplet formation was not observed when the samples were observed in a hot stage of an environmental SEM because the acid evaporated. This effusion of the excess stearic acid from the bilayer intercalated LDHs proceeds in stages. It starts with the removal of interlayer water and terminates in a monolayer-intercalated clay residue. These observations imply that dispersion of LDH-fatty acid in polymer matrices perhaps do not follow the conventional exfoliation or delamination routes. The exudation of stearic acid has implications for the processing behaviour and the dispersion of the clay in the polymer. It was therefore of interest to compare melt blending of LDH-CO_3 and LDH-fatty acid in polymer matrices with varying polarity, e.g. poly(ethylene-co-vinyl alcohol) (EVAL), poly(ethylene-co-vinylacetate) (EVA) and linear low density polyethylene (LLDPE).

2 Experimental

2.1 Materials

The layered double hydroxide (LDH-CO_3) Hydrotalcite HT-5 was supplied by Nkomazi Chemicals, South Africa. LLDPE grade HR411 (density of 0.939 g cm^{-3}; MFI 3.5 g/10 min @ 190 °C/2.16 kg) was obtained from Sasol Polymers, South Africa. EVA grade EV101 was supplied by APC (density 0.941 g cm^{-3}, MFI 1.8 g/10 min @ 190 °C/2.16 kg). EVAL grade EVAL T101B was obtained from Kuraray, Belgium (density 1.17 g cm^{-3}; MFI 1.7 g/10 min @ 190 °C/2.16 kg). Technical grade stearic acid was supplied by Croda Chemicals, UK. Anhydrous ammonia solution was supplied by Merck. Tween 60 (polyoxyethylene-20-sorbitan monostearate) was obtained from Merck.

2.2 Methods

2.2.1 Preparation of LDH-stearate (LDH-St)

The stearate intercalated layered double hydroxide (LDH-St) was prepared according to the method of Nhlapo *et al*. [Nhlapo *et al.,* 2008]. A typical intercalation procedure was carried out as follows. A quantity of 20 g LDH-CO_3 was used in each intercalation reaction. 40 g of surfactant (Tween 60) was dispersed in 1.5 L of distilled water preheated to 80 °C. Excess stearic acid (0.384 mol) was added in a three parts over a period of three days. The mixture was kept at 80 °C for 8 h and allowed to cool to room temperature overnight. The process was repeated over four days with continuous stirring. On the fourth the day no acid was added. The pH of the mixture was maintained at 9.5 ± 0.5 by adding ammonia solution, with each correction carried out once each day. The reaction mixture was allowed to cool. The solids were separated by centrifugation, washed once with water and three times with ethanol and once with acetone. The LDH-St solids were dried at room temperature.

2.2.2 Preparation of composites

The polymer composite containing 10 wt% of either the pristine or the modified LDH were prepared by melt compounding. A TX28P 28 mm co-rotating twin screw extruder with a screw diameter of 28 mm and an L/D ratio of 18 was used. The screw design comprised intermeshing kneader elements with a forward transport action. The screw speed was 170 rpm and the temperatures increased from 100 °C at the feed point to 220 °C at the die. The extruded strands were cooled by passing through a water bath, granulated and dried overnight at 60 °C. Type IV ASTM dumbbells were injection moulded using an Engel 3040 injection-moulding machine with a clamping force 350 kN. The temperature profiles from hopper to nozzle were 200/210/220/220 °C for the LLDPE and EVAL composites and 140/150/160/170 °C for the EVA composites respectively.

2.3 Characterisation

Powder samples were viewed on a JEOL 840 JSM SEM scanning electron microscope. They were prepared as follows; a small quantity of the LDH-St and the LDH-CO_3 precursor was placed onto carbon tape on an aluminium sample holder. Excess powder was removed using a single compressed air blast. Composite samples were cryogenically fractured in liquid nitrogen. They were coated three times with gold under argon gas using the SEM autocoating unit E5200 (Polaron equipment LTD). Imaging of freeze-fractured surfaces was carried out in a JEOL 5400 SEM. The side-view of impact test specimen was imaged on a Zeiss Stereo, Discovery V20 optical microscope.

The clay dispersion within the polymer was studied using a JEOL 2100F transmission electron microscopy (TEM) at an acceleration voltage of 200 kV. The samples were sliced with a diamond knife at -80 °C using a Leica-Reichert Ultracut R with EMFCS cryo-attachment to a nominal thickness of about 90 nm. Each section was mounted on a 300 mesh copper/palladium grid and viewed.

Thermogravimetric analysis was conducted on a Mettler Toledo A851 TGA/SDTA device. Powder samples (ca. 10 mg) were placed in open 70 μl alumina pans. Temperature was scanned at 10 °C min^{-1} in air from 25 to 700 °C.

Differential scanning calorimetry (DSC) data was collected on a Mettler Toledo DSC 1 instrument. Approximately 8 mg samples were placed in aluminium pans. A pin hole was made in the lid. The samples were heated from 0 to 250 °C at a scan rate of 10 °C min^{-1} in N_2 flowing at a rate of 50 mL min^{-1}.

Visco-elastic behaviour was studied with a Perkin Elmer DMA 8000 dynamic mechanical analyzer (DMA) using the single cantilever bending mode. The applied frequency was 1 Hz. The temperature was scanned at 2 °C min^{-1} from -20 °C to 180 °C, -80 °C to 150 °C and -50 °C to 80 °C for EVAL, LLDPE and EVA respectively.

Melt flow viscosity was determined with a Göttfert High Pressure Capillary Rheograph 2000 rheometer. The capillary die had a 180 ° entrance angle and was 30 mm long. The diameter of the capillary was 1 mm. Measurements were done at 190 °C shear rates ranging from 1 s^{-1} to 5000 s^{-1}.

Phase identification was carried out using X-ray diffraction (XRD) analysis on a PANalytical X-pert Pro powder diffractometer. The instrument featured variable divergence and receiving slits, with an X'celerator detector using Fe filtered CoKα radiation (0.17901 nm). The X'Pert High Score Plus software was used for data manipulation.

Tensile testing was carried out on a Lloyds Instruments LRX Plus machine according to ASTM D 638 using Type IV dumbbells. Five specimens were tested for each compound. Charpy impact testing was carried out on a Zwick Impact Tester using the 0.5 J hammer. Tensile impact tests were carried out according to ASTM D1822-06 on Type S and L test specimens.

3. Results and Discussion

The principal factor distinguishing the two fillers, considered presently, is the nature of their planar outside surfaces. The LDH-CO_3 features sheets with exposed hydroxyl groups. Strong hydrogen bonding with the alcohol groups present in the EVAL should be possible. However, these highly polar surfaces would be incompatible with the nonpolar LLDPE matrix. In the case of the LDH-St, the particles are at least partially covered by stearate anions [Focke et al. 2009]. This surface modification with aliphatic chains should provide for improved compatibility with the aliphatic LLDPE chains. As second consideration is the strength of interactions within the clay interlayers. The high charge density and the hydrophilicity of the layers in LDH-CO_3 prevent effective dispersion/exfoliation [Adachi-Pagano *et al.* 2000, Leroux *et al.* 2001, Hibino *et al.* 2001]. In the LDH-St the fatty acid chain

ends in the bilayers only interact via weak van der Waals forces. It should be much easier to delaminate and disperse this clay in polymer matrices.

The degree of clay layer separation in the modified LDHs and the clay dispersion in the polymer composite was studied by X-ray diffraction (Fig. 1). The 2θ values of 13.5 and 27.2 ° typical for LDH-CO_3 indicate a d-spacing (d_L) of 0.76 nm. These reflections were also observed in the LDH-St providing evidence for incomplete conversion. They were also present in all the LDH-CO_3 and LDH-St polymer composites indicating that this clay phase was either retained during melt compounding or more of it generated by decomposition of the LDH-St. The diffractogram for LDH-St showed three basal reflections positioned at 2.0 °, 4.1 ° and 6.1 ° corresponding to a d-spacing of 5.1 nm and consistent with bilayer intercalation [Nhlapo *et al.* 2008; Carlino 1997; Xu and Braterman 2010]. These reflections were absent in the diffractograms of the LDH-St composites. The first reflection observed at higher 2θ values indicates a reduction in the d-spacing of the LDH-St in EVA and EVAL composites (Fig. 1(b). The interlayer spacing of 3.1 nm noticed in the EVAL composite is consistent with monolayer stearic acid intercalated LDH [Xu and Braterman 2010; Braterman et al., 2004]. This collapse in the d-spacing implies that the neutral stearic acid molecules initially present in the interlayer beyond the AEC were removed during the melt compounding process. As discussed in the introduction this was expected in view of the results obtained by Nhlapo et al. [Nhlapo et al. 2008]. A collapse was also observed in the d-spacing value for the clay in the EVA composite. However, the d-spacing was lower and this could be due to a less ordered arrangement of the intercalated chains and/or the loss of the interlayer water. Only vestiges of the LDH-St reflections were seen in the LLDPE composite. Finally, reflections typical for LDH-CO_3 were present in all composite diffractograms. We attribute this to the impurity of the LDH-St but it is possible some could have formed by decomposition of the LDH-St. The XRD data indicated that the LDH based polymer composites contained two types of filler particles (LDH-CO_3 and monolayer stearate intercalated LDH) dispersed within the polymer matrices.

The neat polymer samples had basal reflections at 2θ values of 23.4 °, 24.7 ° and 25.0 ° for EVAL, EVA and LLDPE respectively. In the composites these peaks appear to be broader and of reduced intensity. This indicates that the incorporation of LDHs changed the crystal morphology and increased the disorder in the polymer matrix.

SEM micrographs of the fillers and TEM images of composites are shown in Fig. 2 and Fig. 3 respectively. The pristine LDH-CO_3 powder consisted of small agglomerated platelets, with a sand rose morphology. The stearate modified LDH featured much larger platelets ranging into the 10 μm size. They were also less agglomerated than the LDH-CO_3 particles.

The LDH-CO_3 composites featured distinct as well as agglomerated particles in the sub-micrometer range (Fig. 3). In the LDH-St composites the coarser particles appeared as much smaller planar tactoids with a length up to about 500 nm but with a thickness less than 100 nm (Fig. 3). This considerable reduction in dimensions has two possible explanations. It could be that partial delamination occurred during the high-shear compounding process. LDH platelets are weaker and less rigid than smectite clays and hence more prone to fracture under the high shear action [Solin et al., 1995]. The EVA and LLDPE matrices of the LDH-St composites appeared to contain very few tactoids. In conclusion, the TEM results showed that micro-composites and nanocomposites were obtained using LDH-CO_3 and LDH-St as fillers in the polymer matrices considered.

Fig. 4 to Fig. 6 shows SEM images that give a view of the general morphology and texture of freeze-fractured surfaces. Poor interfacial adhesion is evident in both the LLDPE composites (Fig. 4). This is also the case for the EVA/LDH-CO_3 composite. In all the other samples there was good adhesion between the matrix and the filler as shown by the absence of cavities previously occupied by particles. Some spherical cavities are seen in all the EVAL samples including the neat polymer. However, they are attributed to volatilization of residual water during the moulding process.

Thermal decomposition of layered double hydroxides normally followed three distinct decomposition steps (Fig. 12) [Miyata & Okada 1977, Reichle 1985, Rey *et al.* 1992]. The first event is usually assigned to the loss of physisorbed and interlayer water. The onset of this step is at about 50 °C and is perceived to be completed by 150 °C [Carlino & Hudson 1994, Kandare *et al.* 2006, Frost *et al.* 2003]. The second step is due to a dehydroxylation process immediately followed by an oxidative degradation of the organic anions within the interlayer. The former occurs at about 280 °C and the latter above 450 °C. The breakdown of the hydroxyl lattice and degradation of anions commences at temperatures above 280 °C well above polymer processing temperatures. Mass loss is effectively complete at 700 °C. Intercalation of stearic acid with the LDH interlayer greatly improves its thermal stability. The mean inorganic content of the LDH-St samples prepared in this study was 20 wt%.

Fig. 11 reports the melt viscosity at 190 °C results for the composites. All the samples showed strong shear-thinning behaviour. The EVA and EVAL polymer/LDH-CO_3 composites featured higher apparent viscosity values than the parent polymers. The apparent viscosity of the LLDPE/LDH-CO_3 composite was marginally higher than that of the neat polymer. This is attributed to weak interactions between the polar filler surface and the nonpolar matrix. The apparent viscosities of the EVA and the LLDPE polymer/LDH-St melts were lower than that of the neat polymers. This is attributed to the lubricating effect of the exuded stearic acid.

In the EVAL composites, the LDH-St filler caused the highest increase in the melt viscosity. This means that the interaction of the filler with the polymer chains must have overwhelmed the lubricating effect of the stearic acid. The surfaces of the LDH-St filler are at least partially covered with the chains of the electrostatically attached stearate anions. So it is expected that the interaction with the EVAL chains would be less than the interaction with the uncoated surfaces of the LDH-CO_3 particles. However, the melt viscosity of the LDH-CO_3 composite was lower despite its higher surface polarity. Furthermore, according to the TG results, the inorganic content of the LDH-St is only 20 wt%. In aggregate, these observations

suggest that the interfacial area available for interaction with the polymer chains must have been much higher for LDH-St.

Differential scanning calorimetry (DSC) was employed to study the thermal transitions in the composites (see Fig 13. and Table 2). The data presented pertains to results obtained from first cooling and the second heating run. Both fillers acted as nucleating agents for LLDPE and EVA as the crystallization onset temperature increased (Fig. 13). The degree of crystallinity in the EVA even improved as shown by the increase in the enthalpy of crystallization [Ramaraj and Yoon 2008]. The same fillers retarded the crystallization of the EVAL (Fig. 13). This is attributed to a strong interaction of the EVAL polymer chains with the well-dispersed clay platelets and the higher melt viscosity that suppressed the diffusion processes required for the chains to orient and pack into crystallites.

Fig. 8 to Fig. 10 report DMA visco-elastic properties of the composites. The storage moduli (E′) of the all the LLDPE (Fig. 8), EVA (Fig. 8) and EVAL composites (Fig. 10) were slightly higher than that those of the neat polymer indicating that the incorporation of the filler resulted in a stiffer material. The stiffening effect was more pronounced in the rubbery region than in the glassy region for EVA and EVAL composites. However at higher temperatures the LLDPE/LDH-St deviated from the LDH-CO_3 composite trend and approached the behaviour of the neat polymer. This could be explained by the melting of the excess interlayer stearic acid present and its acting like a plasticizer and lubricant facilitates the motion of the polymer chains.

The glass transition temperature (T_g) of the EVA composites was the same as that of the neat polymer. However, the T_g of the EVAL composites shifted to higher temperatures. There are two possible explanations for this observation when the LDH-St composite is considered. The exuded stearic might have had an anti-plasticization effect or the mobility of the EVAL polymer chains might have been be affected by strong interactions with the surface of the filler particles. Clearly only the latter explanation can hold for the LDH-CO_3 composite as no stearic

acid is present. Based on the viscosity behaviour of the EVAL/LDH-St composite, it can be concluded that this explanation also holds for this system.

Mechanical properties are reported in Table 1. All the filled samples, except the EVAL/LDHSt composite featured higher tensile moduli than the neat polymers. Both LDHs fillers had a reinforcing effect on EVA and LLDPE as both the yield strength and the modulus increased. Better elongations were obtained in the EVA composites but a decrease was observed for the EVAL and LLDPE composites.

Polymer toughness is governed by parameters such as the degree of particle dispersion within the polymer matrix, filler mobility, delamination and intrinsic changes to polymer properties promoted by the filler [Chen 2008]. Tensile impact properties of the filled EVA composites were better that those of the neat polymer. However, the opposite was true for the other polymer matrices. With the exception of the EVAL/LDH-St composite, all composite samples had worse notched Charpy impact properties than the parent polymers. Development of strong energy dissipation mechanisms are a prerequisite for good impact properties. The poor interface adhesion between both fillers and the polyethylene matrix is evident in Fig. 4. This means that the incorporation of the fillers led to the creation of internal flaws. These acted as stress concentrators that lead to premature mechanical failure. The LLDPE/LDH-St composite had slightly better impact strength properties than the LLDPE/LDH-CO_3. This can be attributed to the slightly better compatibility with the polymer matrix contributed by the fatty acid coating on the filler particles (Fig. 4c). However, it is clear from the XRD diffractogram (Fig. 1) that the presence of this filler also affected the morphology of the parent polymer. This is confirmed by the broadening and shift in the position of main reflection attributable to the polymer matrix. This change in the morphology of the polymer matrix could also have affected the impact properties.

The EVA composites did not fracture in the notched Charpy tests because of the rubbery nature of matrix. The tests were basically carried out at room temperature well above

the T_g of the polymer matrix. In the tensile impact tests the LDH-CO_3 filler gave better results than the LDH-St. See Table 1. Considering Fig. 5, this can be attributed to better interfacial adhesion between the polar filler and the polar EVA matrix. Strong interactions with the filler are equivalent to temporary crosslinks that dissipate energy when ruptured. Gersappe [Gersappe 2002] proposed a theory explanation that may explain the improved tensile impact observed in the EVA/LDH-St composite, relative to the neat polymer, despite minimal interaction between the polymer and filler. Since the clay particles are relatively free to move and rotate inside the cavities, they can align themselves in the direction of the applied stress. During the matrix deformation process the filler is squeezed tight by the cavity walls as it elongates and narrows. The resulting friction forces generate a region of enhanced strength that retards the growth of the cavity and thus delays polymer failure.

Unexpectedly, the notched Charpy impact strength of EVAL increased from 4.9 kJ m^{-2} to 7.9 kJ m^{-2} when 10 wt% LDH-St was added (Table 1). Top-view SEM imaging of the fracture surfaces were inconclusive. They did not reveal a mechanism that could explain the improved impact behaviour. Fig. 7 shows (optical microscope) side-view images of the fracture surfaces of Charpy impact specimens obtained for EVAL composite. The neat EVAL sample and EVAL/LDH-CO_3 composite sample showed clean fractures. In contrast, the EVAL/LDH-St sample showed an extensive damage region that extended deep into the sample. It seems that the presence of the LDH-St particles caused repeated branching of the crack fronts. This dissipates mechanical energy by creating numerous internal fractures with a very large total surface area. It seems that the clay particles arrested incoming crack fronts and transmitted them as multiple crack fronts travelling in different directions. This ability of the LDH-St might derive from their sheet-like nature and random orientation in the glassy matrix. It is noteworthy that the stress whitened damage region was located in a narrow region towards the back of the sample. Extensive stress-whitening is usually also an indication of crazing and/or micro-fibril formation. The white appearance of the crazed region is due to light-scattering.

4. Conclusions

It is clear from the work that a combination of factors contribute to properties observed from fatty acid-intercalated LDH/polymer composites. These include the polarity of the polymer and compatibility to the clay; the state and location of intercalated anions. The observation of filler particles in the TEM micrographs is evidence that the LDH-St partially melts and reforms within the confinement of the polymer matrix. The melting process is envisaged to be followed by the removal of the excess stearate from the interlayer, resulting in a monolayer arrangement as observed in the XRD diffractograms. The exuded stearate anions appear to have both lubricating and plasticizing effects on the matrices. On the other hand the remaining LDH-St continues to act as a filler. Improved mechanical properties mainly impact strength was observed in the EVAL + LDH-St, the difference in the performance is conventionally attributed to strong hydrogen bonding interaction between the -OH groups on the polymer backbone with those on the LDH lattice. Minimal or no interaction is observed in the LLDPE composites. The crystallinity of the polymers seemed to play a very important role with respect to properties observed. The LDH filler appears to act as a nucleating agent for crystallization in the LLDPE composites, the change in crystallisation behaviour could be detrimental to the impact properties

Acknowledgements

This work is based on research supported by the National Research Foundation (NRF) through the Institutional Research Development Programme (IRDP) and the South Africa/Germany Research Collaboration Programme. Financial support from NRF and also from the Bundesministerium für Forschung (BMBF) is gratefully acknowledged.

References

[1] D.R. Paul, L.M. Robeson, Polymer. 49(2008) 3187-3204

[2] S. Pradhan, F.R. Costa, U. Wagenknecht, D. Jehnichen, A.K. Bhowmick, G. Heinrich, Eur. Polym. J. 44 (2008) 3122-3152

[3] H.-B. Hseuh, C.-Y. Chen, Polymer. 44 (2003) 5275-5283

[4] G.-A. Wang, C.-C. Wang, C.-Y. Chen, J. Polym. Degrad. Stab. 91 (2006) 2443-2450

[5] M. Zammarano, M. Franceschi, S. Bellayer, J.W. Gilman, S. Meriani, Polym. J. 46 (2005) 9314-9328

[6] F. R. Costa, M. Abdel-Goad, U. Wagenknecht, G. Heinrich, Polymer, 46 (2005) 4447-4453

[7] W. Chen, B. Qu, Chem. Mater. 15 (2003) 3208-3213

[8] W. Chen, B. Qu, J. Mater. Chem. 14 (2004) 1705-1710

[9] M. Zubitur, M.A. Gomez, M. Cortazar, J. Polym. Degrad. Stab. 94 (2009) 804- 809

[10] S. Bocchini, S. Morlat-Therias, J. L. Gardette, G. Camino. Eur. Polym. J. 44 (2008) 3473-3481

[11] B. Magagula, N. Nhlapo, W. W. Focke, J. Polym. Degrad. Stab. 94 (2009) 947-954

[12] A. Manhique, W.W. Focke, Mol. Cryst. Liq. Cryst. 554 (2012)

[13] W.T. Reichle, Chemtech, (1986) 58-63

[14] W.J. Work, K. Horie, M. Hess, R.F.T. Stepto, Pure Appl. Chem. 11(2004)1985-2007

[15] G. Huang, A. Zhuo, L. Wang, X. Wang, Mater. Chem. Phys. 130 (2011) 714-720

[16] W.D. Lee, S.S. Im, J. Polym. Sci., Part B: Polym. Phys. 45 (2007) 28-40

[17] E. M. Moujahid, J.-P. Besse, F. Leroux, J. Mater. Chem. 12 (2002) 3324-3330

[18] B. Ramaraj, S. K. Nayak, K.R. Yoon, J. Appl. Polym. Sci. 116 (2010) 1671-1677

[19] M. Zammarano, S. Bellayer, J.W. Gilman, M. Franceschi, F.L. Beyer, R.H. Harris, S. Meriani, Polymer. 47 (2006) 652-662

[20] R.A. Vaia, E. P. Giannelis, Macromolecules. 30 (1997) 8000-8009

[21] R.A. Vaia, E. P. Giannelis, Macromolecules. 30 (1997) 7990-7999

[22] H. Fischer, Mat. Sci. Eng. C. 23 (2003) 763-772

[23] F. Leroux, M. Adachi-Pagano, M. Intissar, S. Chauvière, C. Forano, J-P. Besse, J. Mater. Chem. 11 (2001) 105-112.

[24] A. Khan, D. O'Hare, J. Mater. Chem. 12 (2002) 3191-3198.

[25] J. Liu, G. Chen, J. Yang, L. Ding, J. Mat. Chem. Phys. 118 (2009) 405-409

[26] C. Nyambo, D. Wang, C.A. Wilke, Polym. Adv. Technol. 20 (2009) 332-340

[27] L. Qui, W. Chen, B. Qu, J. Polym. Degrad. Stab. 87 (2005) 433-440

[28] N. Nhlapo, T. Motumi, E. Landman, S. M. C. Verryn, W. W. Focke, J. Mater. Sci., 43-3 (2008) 1033-1043.

[29] W.W. Focke, N.S. Nhlapo, L. Moyo, S.M.C. Verryn, Mol. Cryst. Liq. Cryst. 521 (2010) 168-178

[30] L. Moyo, W.W. Focke, F.J.W. Labuschagne, S.M.C. Verryn, Mol. Cryst. Liq. Cryst. (2012) *Accepted*

[31] P.S. Braterman, Z.P. Xu, F. Yarberry, in: S.M. Auerbach, K. A. Carrado, P.K. Dutta (Eds), Handbook of Layered Materials, CSC Press, Taylor & Francis Group, Boca Raton, 2004, pp. 373-449

[32] S. Carlino, Solid State Ionics, 98 (1997) 73-84

[33] Z.P. Xu, P. Braterman, Appl. Clay Sci. 48 (2010) 235-242

[34] D.F. Eckel, M.P. Balogh, P.D. Fasulo, W.R. Rodgers, J. Appl. Polym. Sci. 93 (2004) 1110-1117

[35] S.A. Solin, D. Hines, S.K. Yun, T.J. Pinnavaia, M.F. Thorpe, J. Non-Cryst. Solids 182 (1995) 212-220

[36] W.W. Focke, D. Molefe, F.J.W. Labuschagne, S. Ramjee, J. Mat. Sci. 44 (2009) 6100-6109

[37] M. Adachi-Pagano, C. Forano and J-P Besse, Chem. Commun. (2000) 91-92

[38] T. Hibino, W. Jones, J. Mater. Chem. (2001) 1321-1323

[39] B. Chen, J.R.G. Evans, H.C. Greenwell, P. Boulet, P. V. Coveney, A. A. Bowden, A. Whiting, Chem. Soc. Rev. 37 (2008) 568-594

[40] D. Gersappe, Phys. Rev. Lett. 89-5 (2002) 58301-5830

[41] S. A. Paul, C. Sinturel, K. Joseph, G.D. Gem Mathew, L.A. Pothan, S. Thomas, Polym. Eng. Sci. (2010) 384-395

[42] S. Miyata, A. Okada, Clays Clay Miner. 25 (1977)14-18

[43] W. T. Reichle, J. Catal., 94 (1985) 547-557.

[44] F. Rey, V. Fornes, J.M. Rojo, J. Chem. Soc., Faraday Trans. 88 (1992) 2233-2288

[45] S. Carlino, M. J. Hudson, J. Mater. Chem. 4 (1994) 99-104.

[46] E. Kandare, J. M. Hossenlopp, Inorg. Chem., 45 (2006)3766-3773.

[47] R. L. Frost, W. Martens, Z. Ding, J. T Kloprogge, J. Therm. Anal. Calorim. 71 (2003) 429-438.

[48] B. Ramaraj, K. R. Yoon, J. Appl. Polym. Sci. 108 (2008) 4090-4095

[49] T.J. Hutley, M. W. Darlington, Polym. Commun. 26 (1985) 264-267

Lists of Tables

Lists of Figures

Table 1
Mechanical properties of LDH/polymer composites

Polymer Composite	Young's Modulus (MPa)	Yield Strength (MPa)	Strain to Break (%)	Charpy Impact Strength (kJ m^{-2})	Tensile Impact Strength (kJ m^{-2})
EVA					
Neat EVA	27 ± 2	10 ± 0.4	277 ± 30	No break	3.8 ± 0.14
EVA + LDH-St	40 ± 5	12 ± 0.1	422 ± 23	No break	4.3 ± 0.19
EVA + LDH-CO_3	37 ± 2	13 ± 1	424 ± 60	No break	5.2 ± 0.06
LLDPE					
Neat LLDPE	171 ± 14	16 ± 0.1	509 ± 29	22 ± 2	1.7 ± 0.08
LLDPE + LDH-St	196 ± 23	17 ± 0.4	495 ± 43	12 ± 1	1.2 ± 0.07
LLDPE + LDH-CO_3	213 ± 12	17 ± 0.2	460 ± 21	11 ± 1	0.8 ± 0.05
EVAL					
Neat EVAL	843 ± 16	64 ± 2	41 ± 21	4.9 ± 1	2 ± 0.28
EVAL + LDH-St	718 ± 40	59 ± 1	18 ± 5	7.9 ± 3	0.8 ± 0.33
EVAL + LDH-CO_3	1025 ± 18	76 ± 0.4	37 ± 2	4.6 ± 1	0.7 ± 0.29

Table 2
DSC data of neat polymer and composites

	Onset Melting temperature (°C)	**Melting Temperature, T_m (°C)**	**Melting Endotherm (J g^{-1})**	**Onset Crystallisation (°C)**	**Crystallisation Temperature, T_c (°C)**	**Crystallisation exotherm (J g^{-1})**
Neat EVA	60	85	55	75	70	55
EVA + LDH-St	60	85	42	76	71	46
EVA + LDH-CO_3	64	85	60	74	70	63
Neat EVAL	176	182	55	164	162	47
EVAL + LDH-St	175	183	48	161	157	46
EVAL + LDH-CO_3	175	181	45	163	161	46
Neat LLDPE	121	126	76	117	115	61
LLDPE + LDH-St	121	127	68	118	116	63
LLDPE + LDH-CO_3	120	128	67	119	117	61

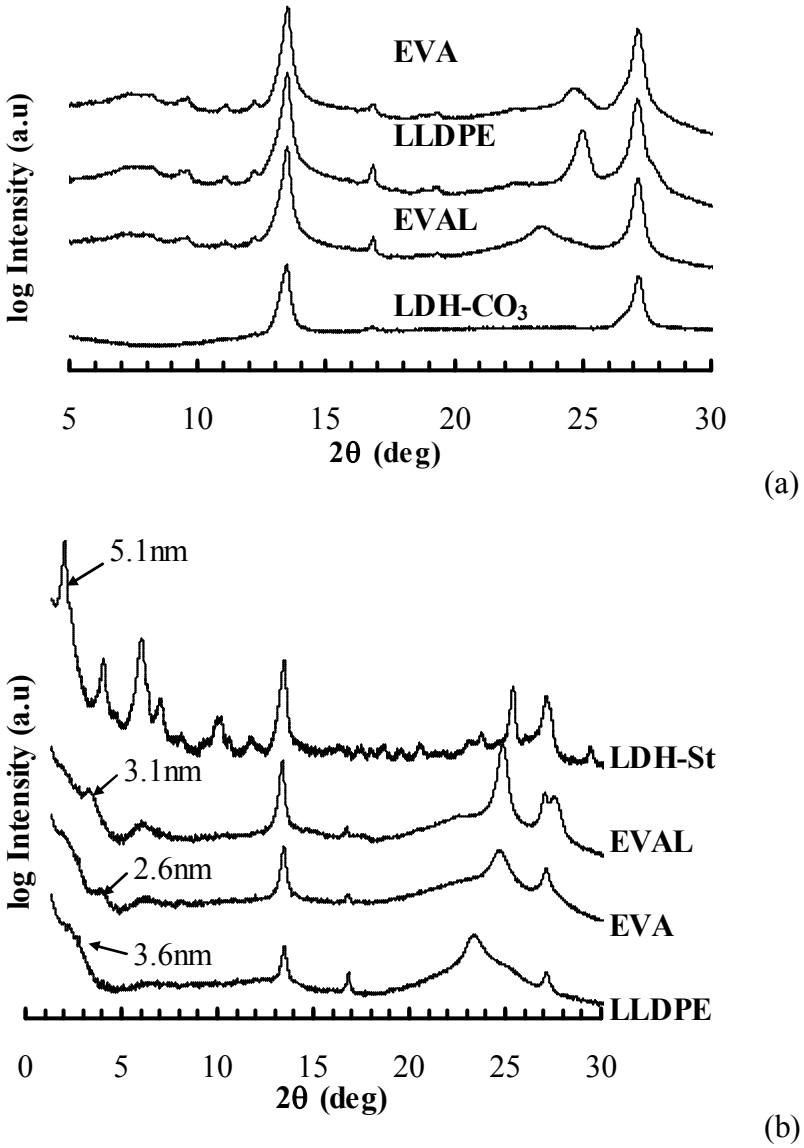

Fig. 1. XRD diffractograms (WAXS) of the pristine, modified LDH and polymer composite indicating the relevant basal spacing

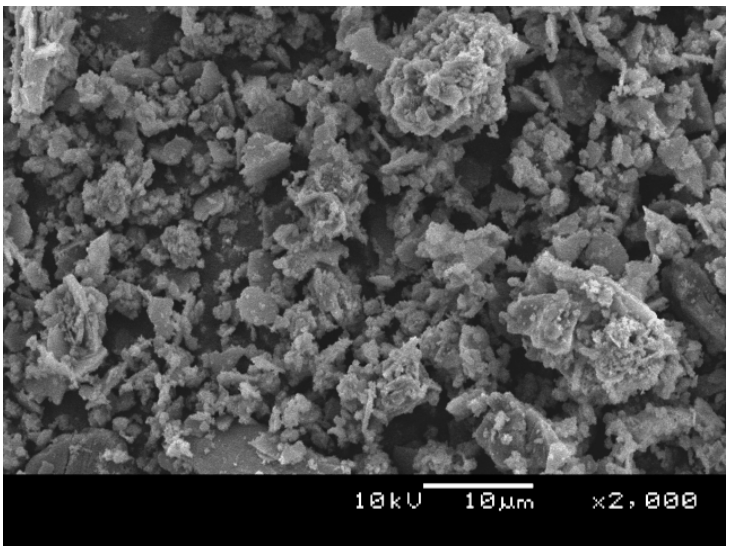

(a)

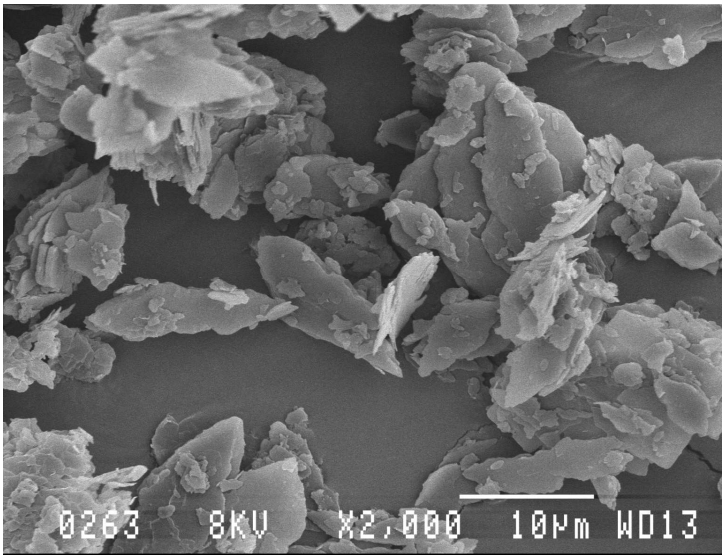

(b)

Fig. 2. SEM micrographs of (a) LDH-CO_3 and (b) LDH-St

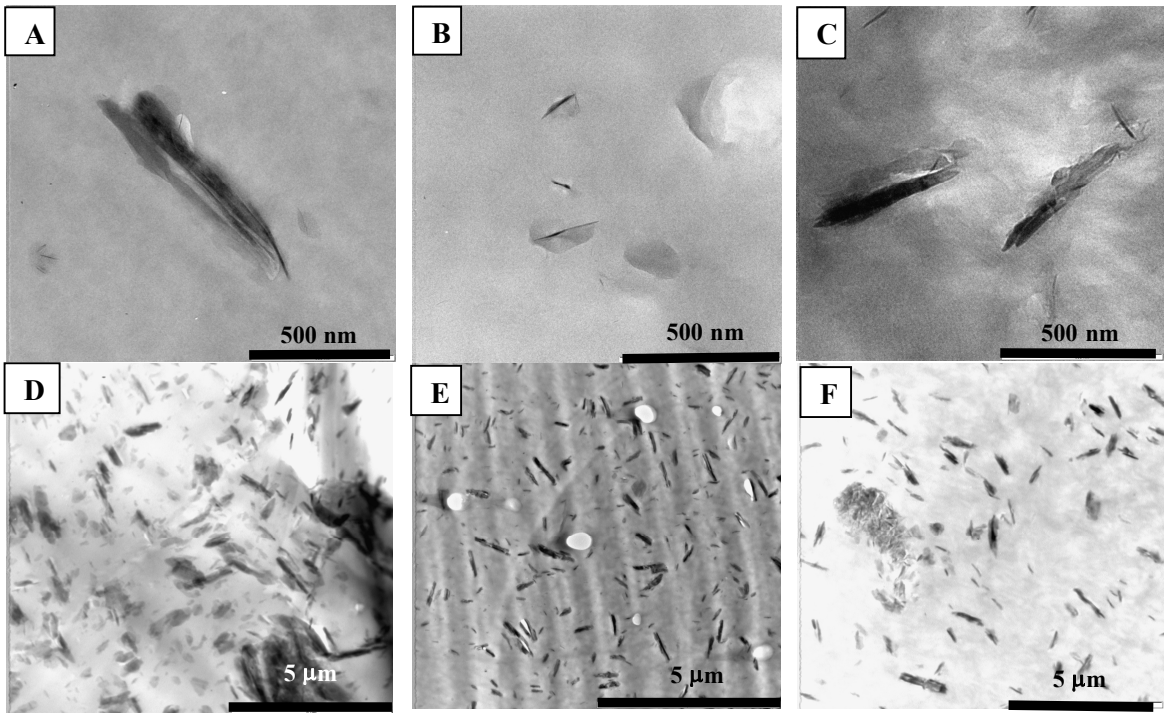

Fig. 3. TEM images of the polymer composites of (a) EVA + LDH-St; (b) EVAL + LDH-St; (c) LLDPE + LDH-St; (d) EVA + LDH-CO_3; (e) EVAL + LDH-CO_3 and (f) LLDPE + LDH-CO_3

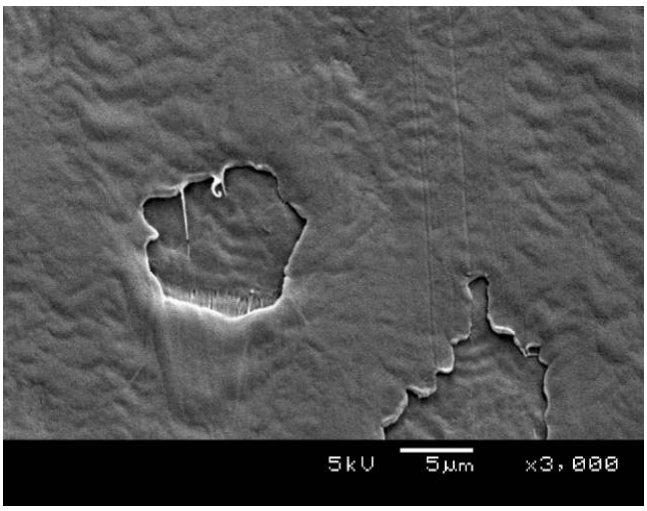

(a)

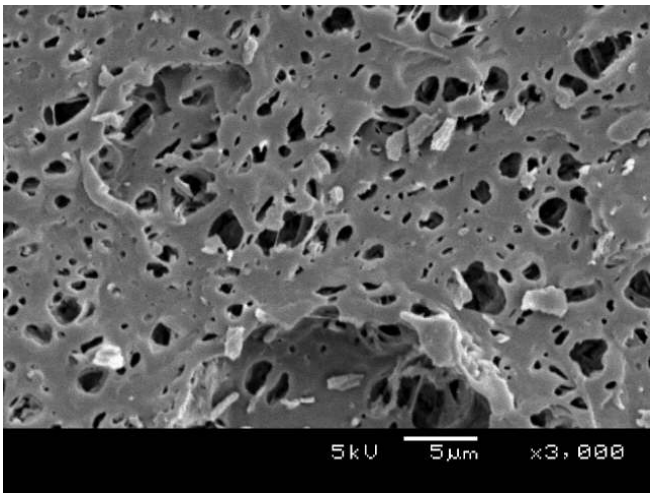

(b)

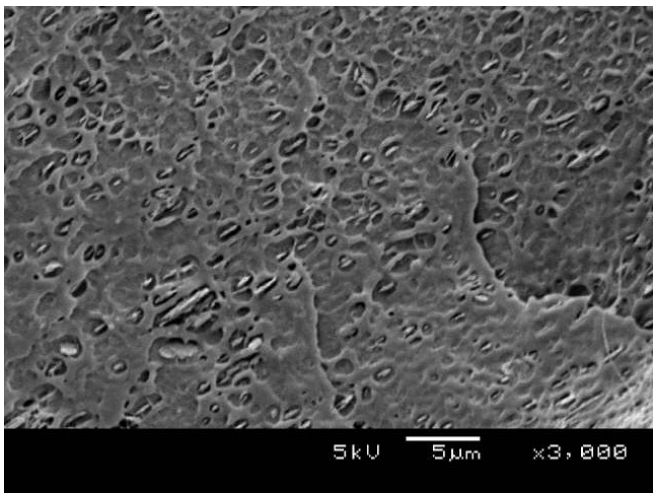

(c)

Fig. 4. Freeze-fractured surface of (a) Neat LLDPE (b) LLDPE + LDH-St and (c) LLDPE + LDH-CO_3

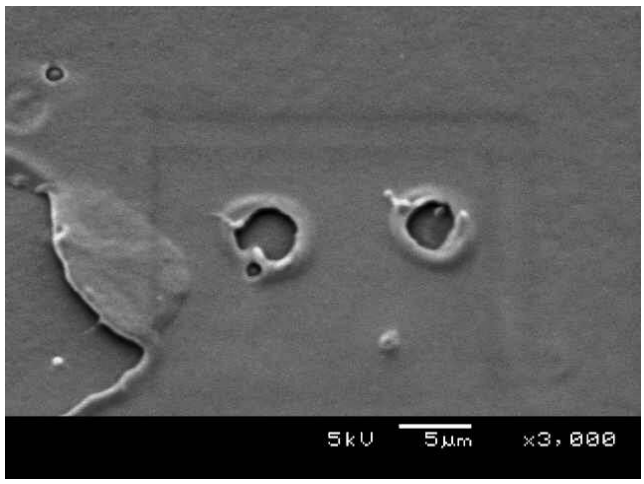

(a)

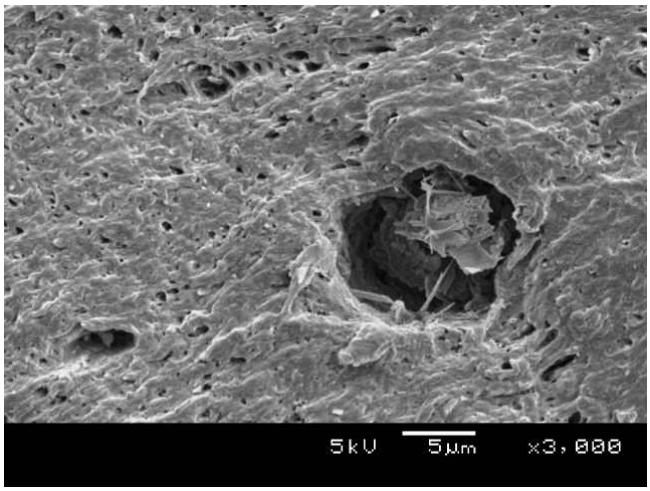

(b)

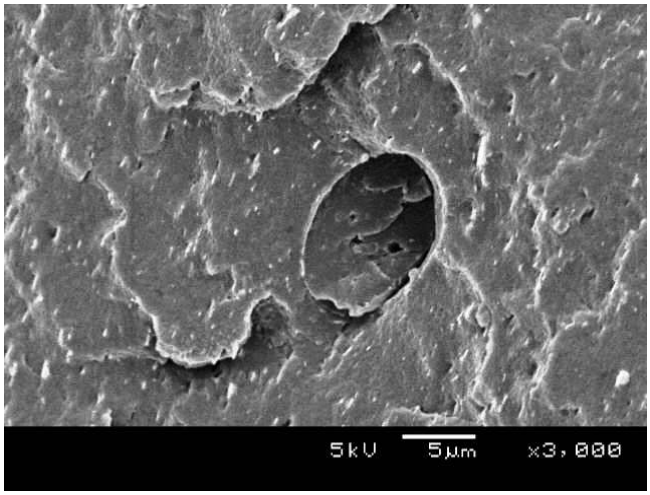

(c)

Fig. 5. Freeze-fractured surface of (a) Neat EVA (b) EVA + LDH-St and (c) EVA + LDH-CO_3

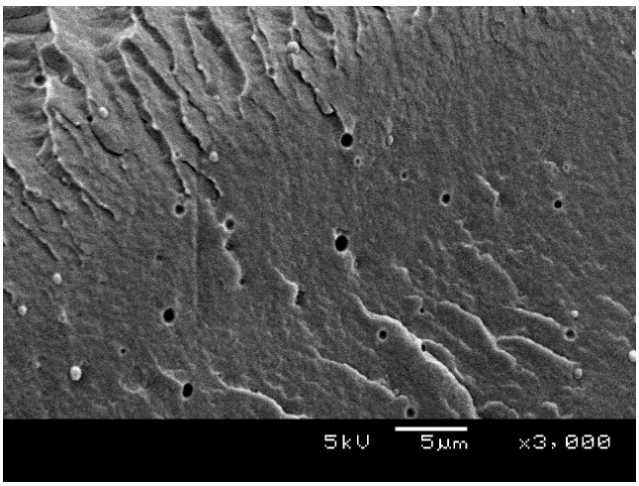

(a)

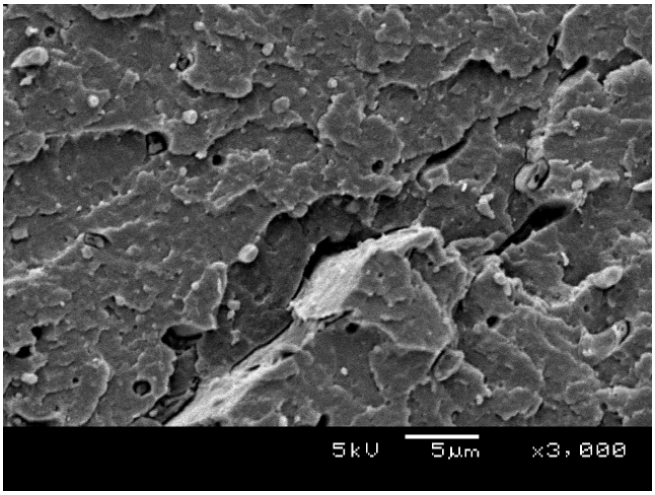

(b)

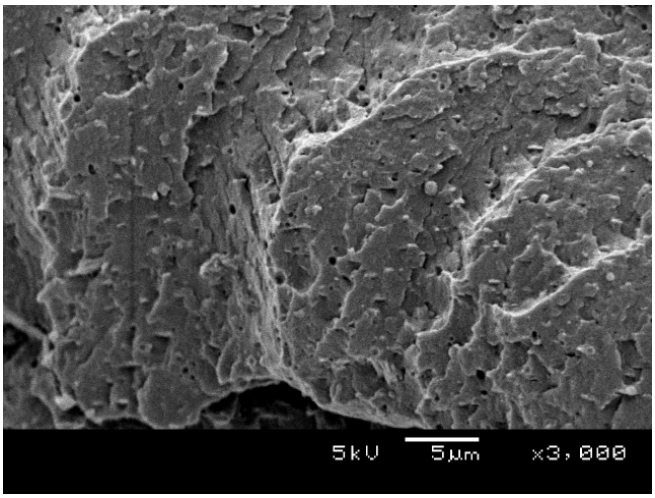

(c)

Fig. 6. Freeze-fractured surface of (a) Neat EVAL (b) EVAL+ LDH-St and (c) EVAL + LDH-CO_3

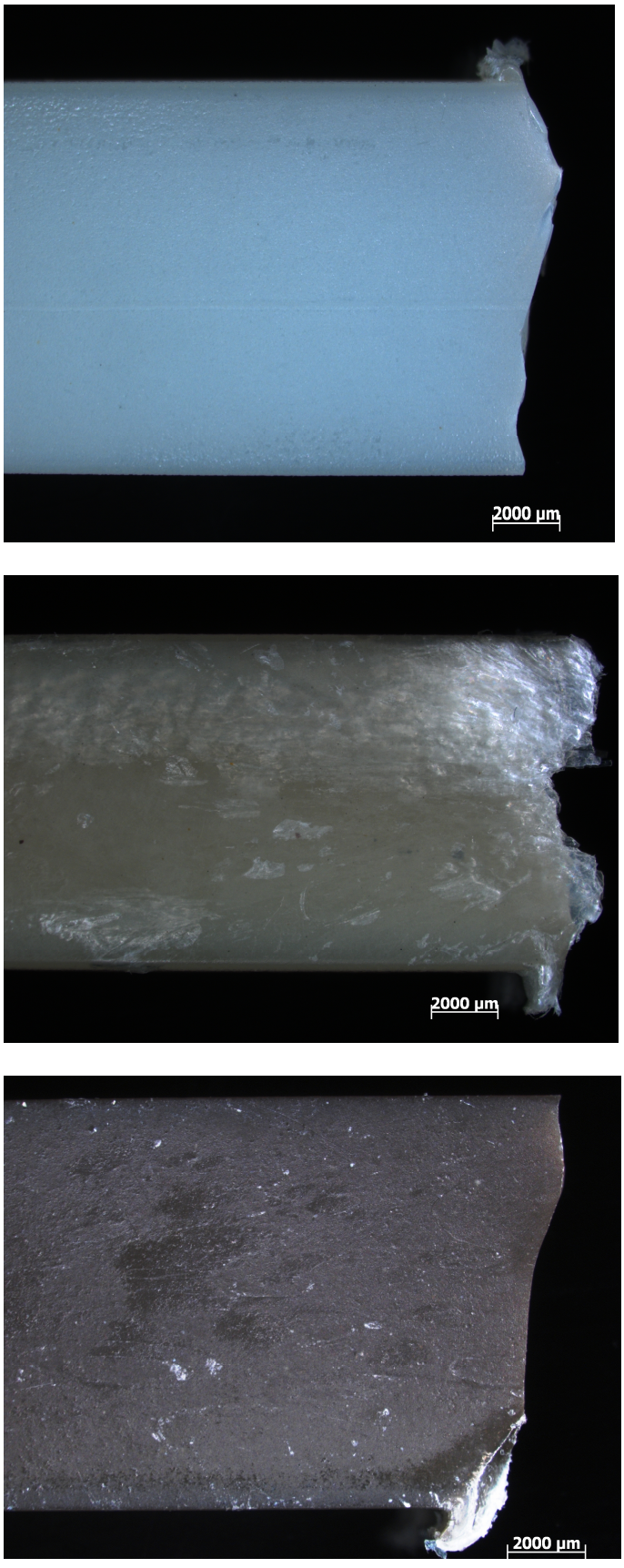

Fig. 7. Side-view of Charpy impact test specimen of EVAL (a) neat, (b) LDH-St and (c) LDH-CO_3 composites

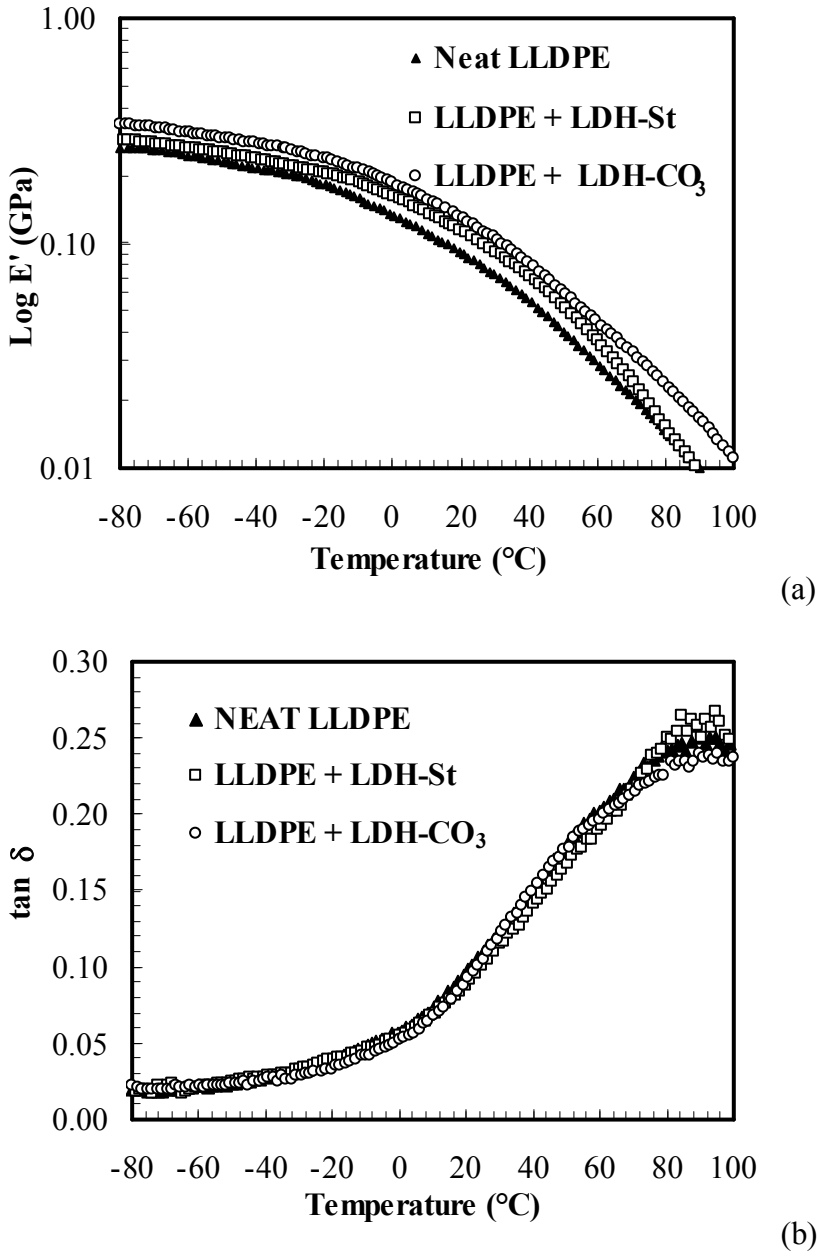

Fig. 8. DMA data for LLDPE and its derivative composites (a) storage modulus, (b) tan δ

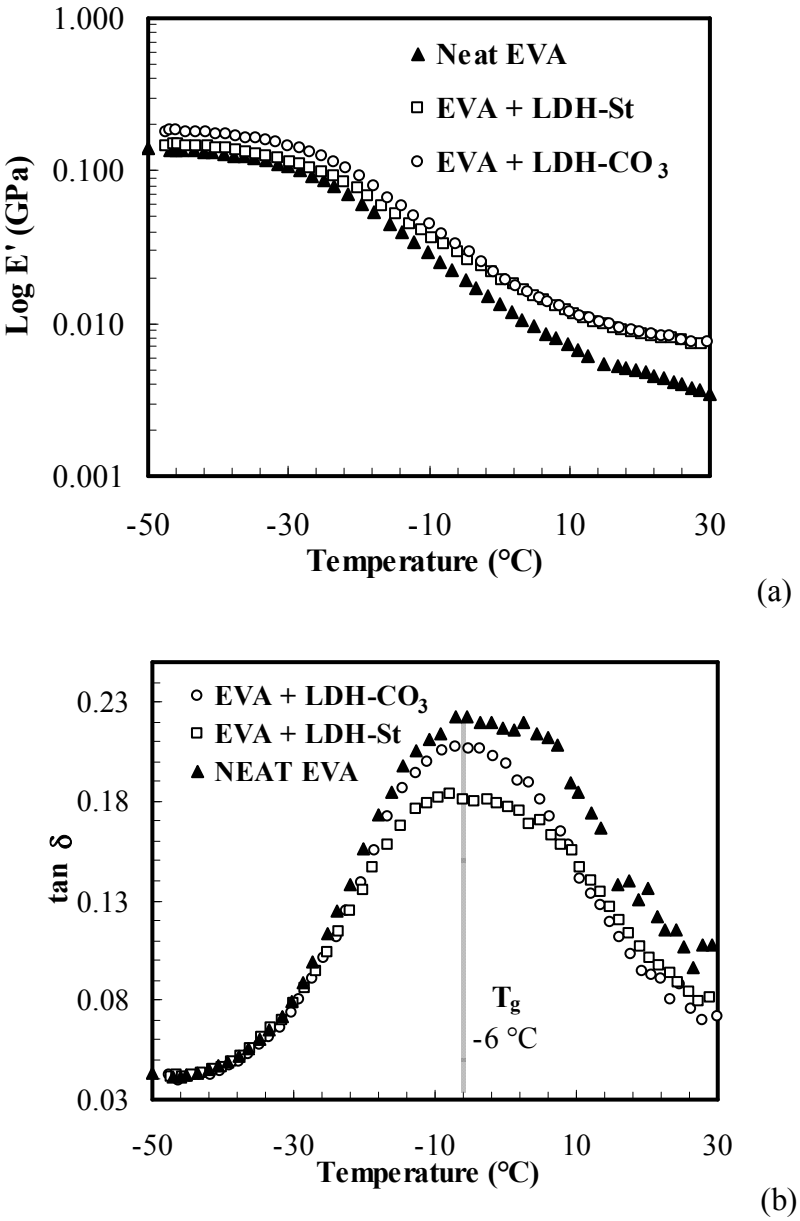

Fig. 9. DMA data for EVA and its derivative composites (a) storage modulus, (b) tan δ

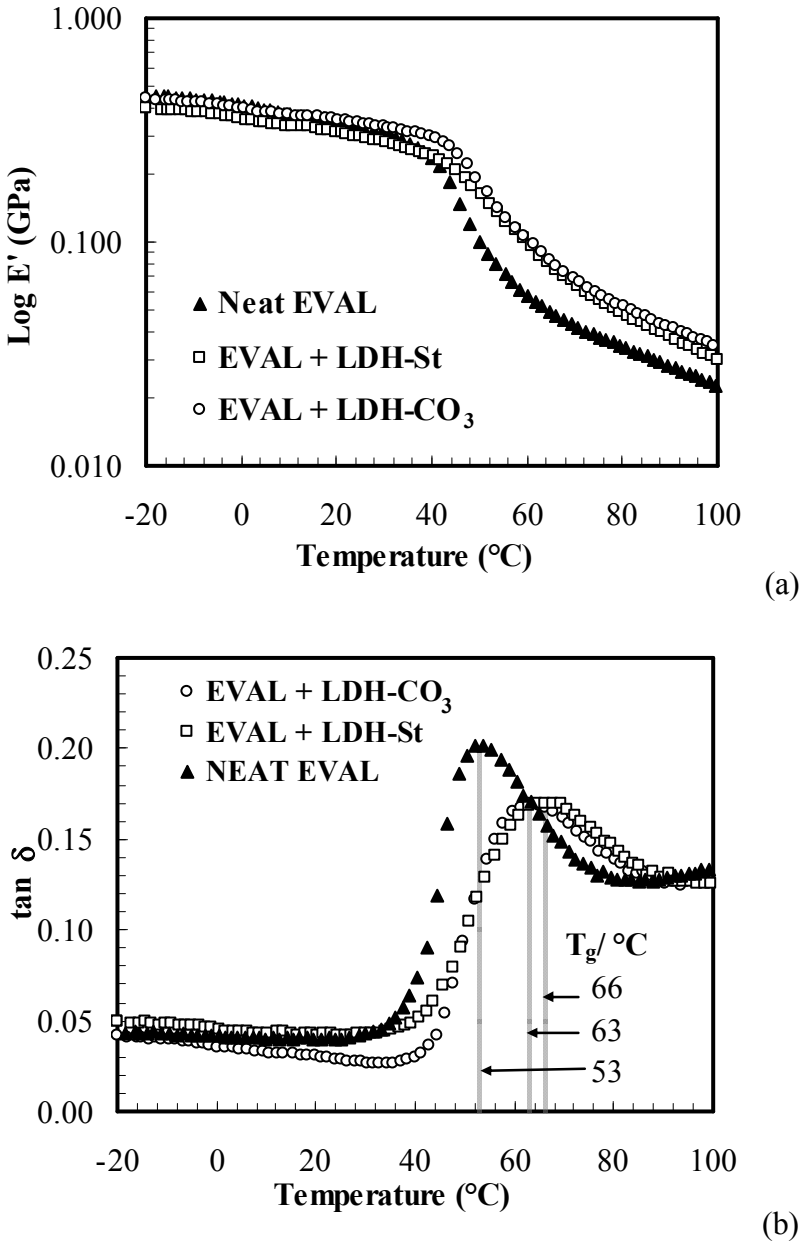

Fig. 10. DMA data for EVAL and its derivative composites (a) storage modulus, (b) tan δ

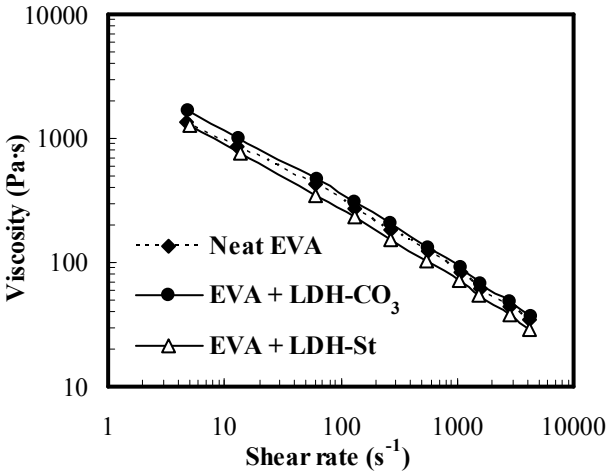

(a)

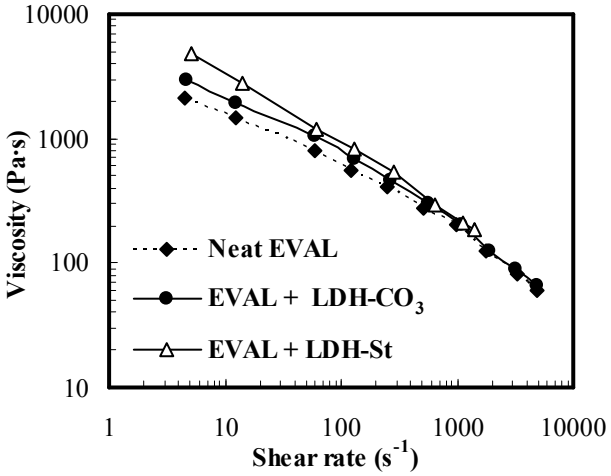

(b)

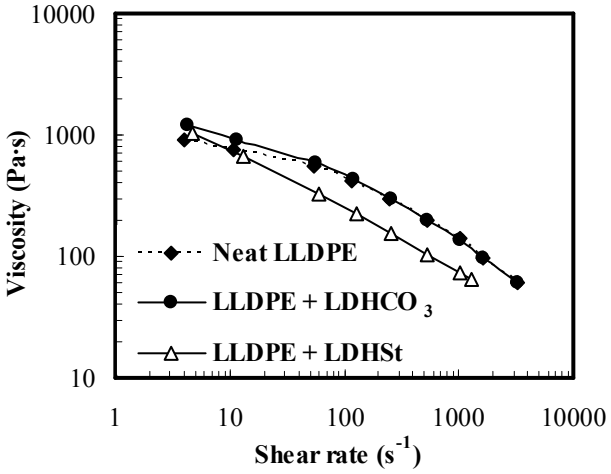

(c)

Fig. 11. Effect of LDH incorporation on viscosity of the polymer (a) EVA (b) EVAL and (c) LLDPE at 190 °C

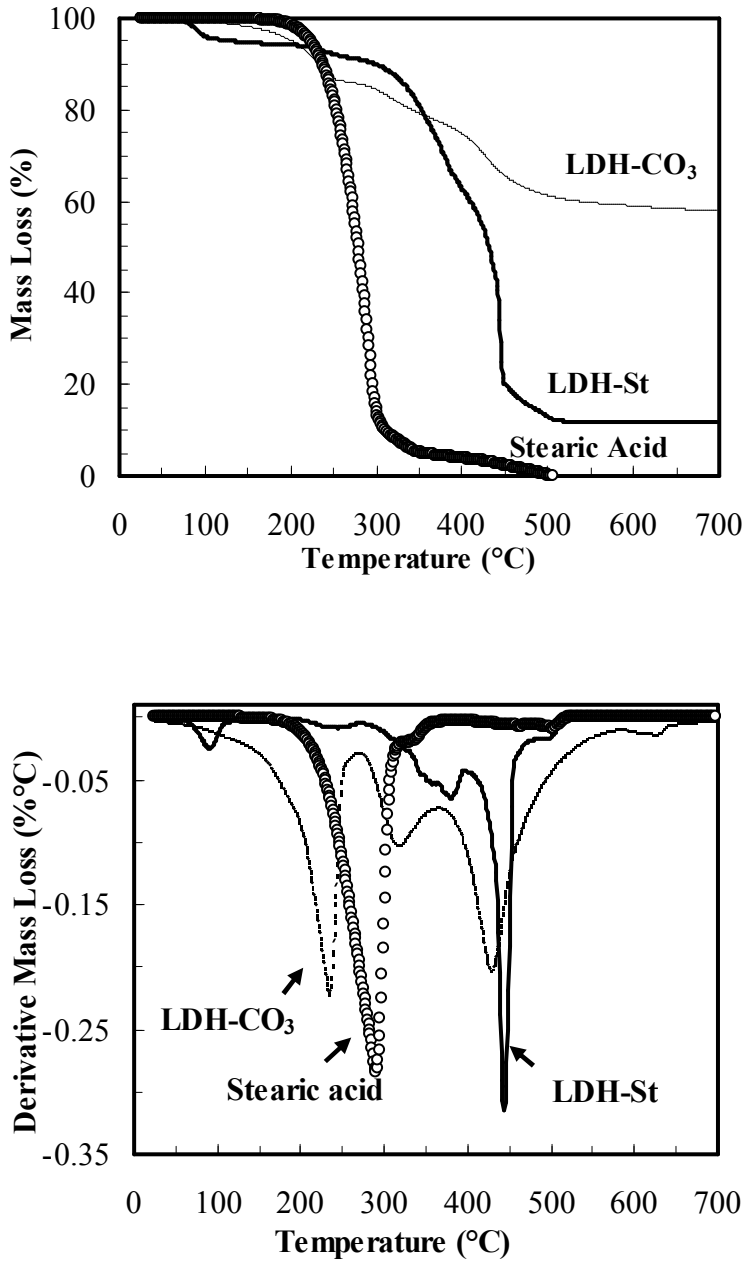

Fig. 12. Thermogravimetric and derivative mass loss curves of LDH-CO_3 and LDH-St

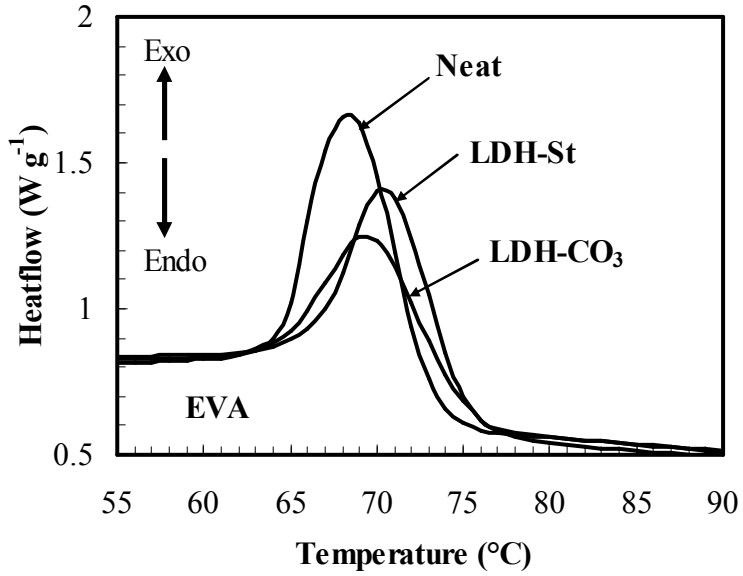

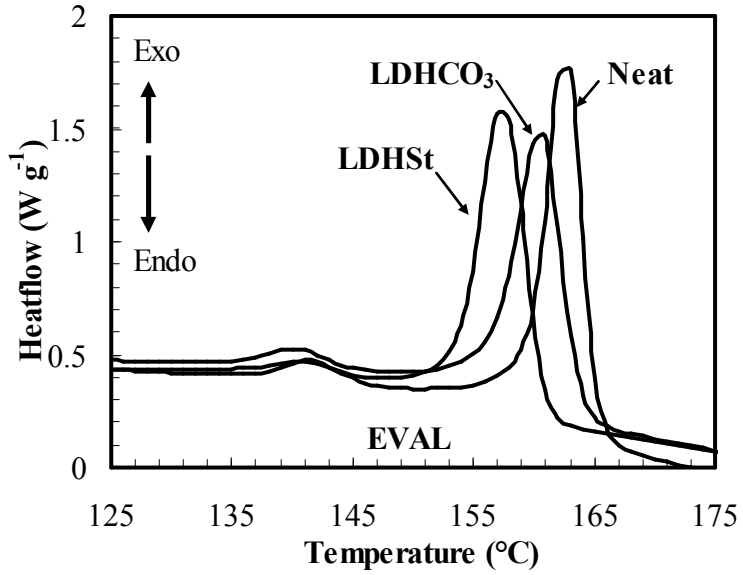

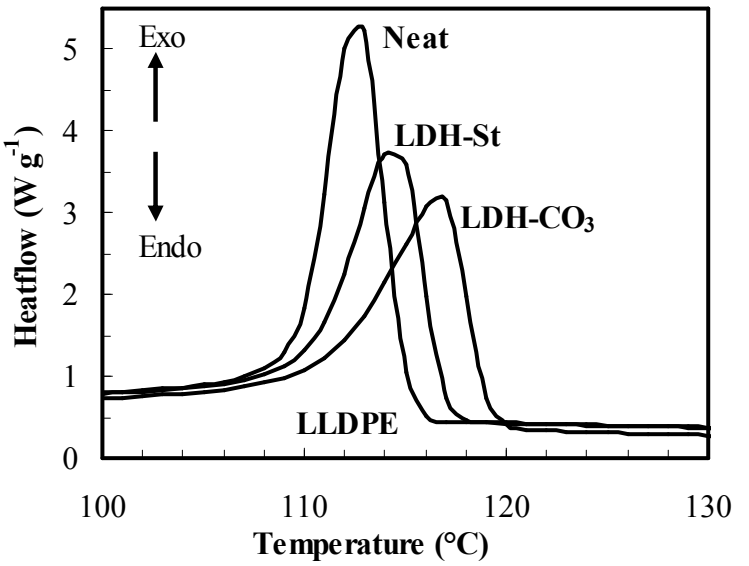

Fig. 13. DSC cooling traces of each polymer composite system